.

AN ANALYSIS OF SALT CONCENTRATIONS IN THE RAINWATERS OF KANEOHE, HAWAIʻI

A THESIS SUBMITTED TO
THE GLOBAL ENVIRONMENTAL SCIENCE
UNDERGRADUATE DIVISION IN PARTIAL FULFILLMENT
OF THE REQUIREMENTS FOR THE DEGREE OF

BACHELOR OF SCIENCE

IN

GLOBAL ENVIRONMENTAL SCIENCE

August 2021

By
Christopher Corpus

Thesis Advisor
Dr. Alison D. Nugent

I certify that I have read this thesis and that, in my opinion, it is satisfactory in scope and quality as a thesis for the degree of Bachelor of Science in Global Environmental Science.

THESIS ADVISOR

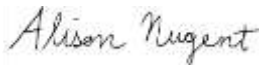

Dr. Alison D. Nugent
Department of Atmospheric Sciences

For my family and friends for always pushing me to be better than I was before.

ACKNOWLEDGEMENTS

The completion of this study would not have been possible without the assistance of Dr. Alison Nugent, my thesis advisor. I would also like to thank Kexin Catherine Rong from the Water Resources Research Center.

In addition, I would like to thank my grandparents, family, and friends for always supporting me and pushing me to be better than I was the day before.

ABSTRACT

Sea spray aerosols (SSA) are a naturally occurring aerosol in marine regions, formed from white-capping and wave breaking along coastlines. SSA are hypothesized to play a significant role in the local climatology of coastal areas by acting as giant cloud condensation nuclei (GCCN), which can accelerate warm rain initiation due to their high hygroscopicity. However, there is large uncertainty about how much SSA mass makes it up into the clouds and participates in precipitation formation. SSA in the atmosphere are also collected by raindrops as they fall, further complicating the issue. To investigate the question of how much SSA is in rainwater, we analyzed the salt content of rainwater on O‘ahu at daily intervals from Kaneohe. We compared the salt content in rainfall to atmospheric variables to see how wind speed, wind direction, humidity, and rainfall play a role through their modulation of rain processes. We found that on average, Sodium and Chloride held a strong inverse relationship with total water mass. However, we found a weak relationship between ion concentration and rain rate with ion concentrations becoming inconsistent at lower rain rates and holding relatively low values with higher rain rates. The goal of this work is a more complete understanding of the concentration of salt in rainwater on O‘ahu and the changes from day to day due to atmospheric variability.

TABLE OF CONTENTS

LIST OF TABLES

LIST OF FIGURES

1.0 INTRODUCTION

1.1 Motivation

Sea salt aerosols (SSA) maintain a significant role in the local climatology of Hawai‘i. SSA is a naturally large aerosol (typically > 1 μm), especially when generated by the tearing of droplets from the top of breaking waves. If able to be lofted to cloud base, the SSA may directly act as cloud condensation nuclei (CCN), rapidly grow, broaden the cloud droplet size distribution, and readily initiate the warm-rain processes (Chen et al. 2007, Jensen and Nugent, 2017). The term ‘warm rain’ refers to rain derived from non-ice phase processes in clouds (Lau et al. 2003). It is formed through the condensational growth, and later coalescence of water droplets that broaden the droplet spectrum causing the droplets to fall at a variety of terminal velocities within the clouds. Warm rain is an integral component of the tropical precipitation system, contributing to heating and moistening of the lower troposphere, modifying stability, and possibly altering the recycling time scales of organized tropical convection (Johnson et al. 1999; Johnson and Lin, 1997; Mapes, 2000; Wu, 2003; Del Genio and Kovan, 2002). As Hawai‘i is a tropical island, the SSA’s may play an important role in the local precipitation system.

SSA are such effective CCN because SSA have high hygroscopicity and cloud droplets formed on SSA grow at an accelerated rate compared to cloud droplets grown on other aerosols. As such, they are hypothesized to speed up the warm-rain process, causing rain to initiate more quickly, and to increase rain rates when it does form. Note that SSA are not expected to play a large role during heavy rain events where clouds extend above the freezing level and clouds are going to rain regardless of aerosol-cloud interactions.

The influence of SSA is likely to be largest during shallow trade cumulus periods, where the presence of SSA may make up the difference between whether a trade cumulus cloud rains or not.

SSA are removed from the atmosphere through gravitational sedimentation, collection by falling raindrops, and through the warm-rain process described earlier. Therefore, not all of the SSA found in the rainwater will have taken part in the warm rain process; some may be from the collection of suspended atmospheric SSA as the raindrop falls to the ground. SSA particles have a significant role in sensitive terrestrial and aquatic ecosystems, causing an alteration of nutrient balances (Greaver et al. 2012; Lehmann et al. 2005). This includes the increase of the salinity of watersheds and other aquatic ecosystems. Extreme weather events that include heavy rain and high winds can also result in significant depositional fluxes of chemical species such as sodium (Na^+) over short periods (Avery et al. 2004). Most notably, tropical storm systems have been shown to be responsible for major depositions of sea salt (Na^+ and chloride, Cl^-) to land (Mallaugh et al. 2012). This study hopes to gain a more complete understanding of SSA in rainwater. Specifically, what factors may affect the concentration of major ion species in rainwater, and what the typical amount of the major ion species in rainwater is under a range of conditions.

1.2 Background

Prior work has been conducted on this topic in Hawai‘i in the 1950s. An experiment conducted on the Big Island studied the chemical composition of rain in the Project shower area from higher altitudes inland near Mauna Kea to the Windward coastline and found that the total salt concentration decreases inland to extremely low values on the upper slopes of the volcanoes (Eriksson 1957). The study found that the rainwater collected on the Island of Hawai‘i is similar in solute concentration to the Swedish west coast (Na^+, K, Mg, Ca, NH_3-N, NO_3-N, Cl^-, and SO_4-S) except for ammonia and nitrate which were very low. If SSA were taking part in the warm rain process and helping to initiate warm rain, this is the expected pattern that would be found; higher concentrations of ions along the coast, decreasing inland as the cloud processes become less dependent on SSA, and as SSA is rained out and continuously depleted from the cloud.

A similar experiment was conducted on the rainwater chemistry over the conterminous United States (Keresztesi et al. 2020). Figure 1a shows a strong sodium gradient with the highest sodium content in rainwater being 61 - 140 μeq L^{-1} found along the coastlines of the U.S suggesting the presence of sea salt in rainwater and decreased sodium content of 4.6 - 7.7 μeq L^{-1} inland which may be due to a blocking effect by the mountainous regions, or the same rainwater fallout away from the coastline as described above. A similar gradient was found in Figure 1b with Chlorine concentrations being 13-65 μeq L^{-1} around the coastlines and 2.9 - 0.94 μeq L^{-1} inland. The Enrichment Factor (EF) calculation in Eq. 1 was utilized as an indicator to assess the presence and intensity

of anthropogenic contaminant deposition (Barbieri 2016). The study found that the enrichment factor given by,

$$EF_{seawater} = [X/Na^{+}]_{rainwater} / [X/Na^{+}]_{seawater} \quad \text{(Equation 1)}$$

of the sea for Cl^- was stronger than the enrichment factor Cl^- of the crust which suggests the majority of Cl^- was sourced from marine sources.

The study utilized Spearman's rank correlation analysis to determine the relative source of the major ionic constituents in precipitation samples (Keresztesi et al. 2020). The correlation analysis considered a correlation coefficient significant if $R > 0.35$ at 95% confidence (Keresztesi et al. 2020). The study found that a strong correlation between Na^+ and Cl^- suggests that the source of the ions was from sea spray and marine salts.

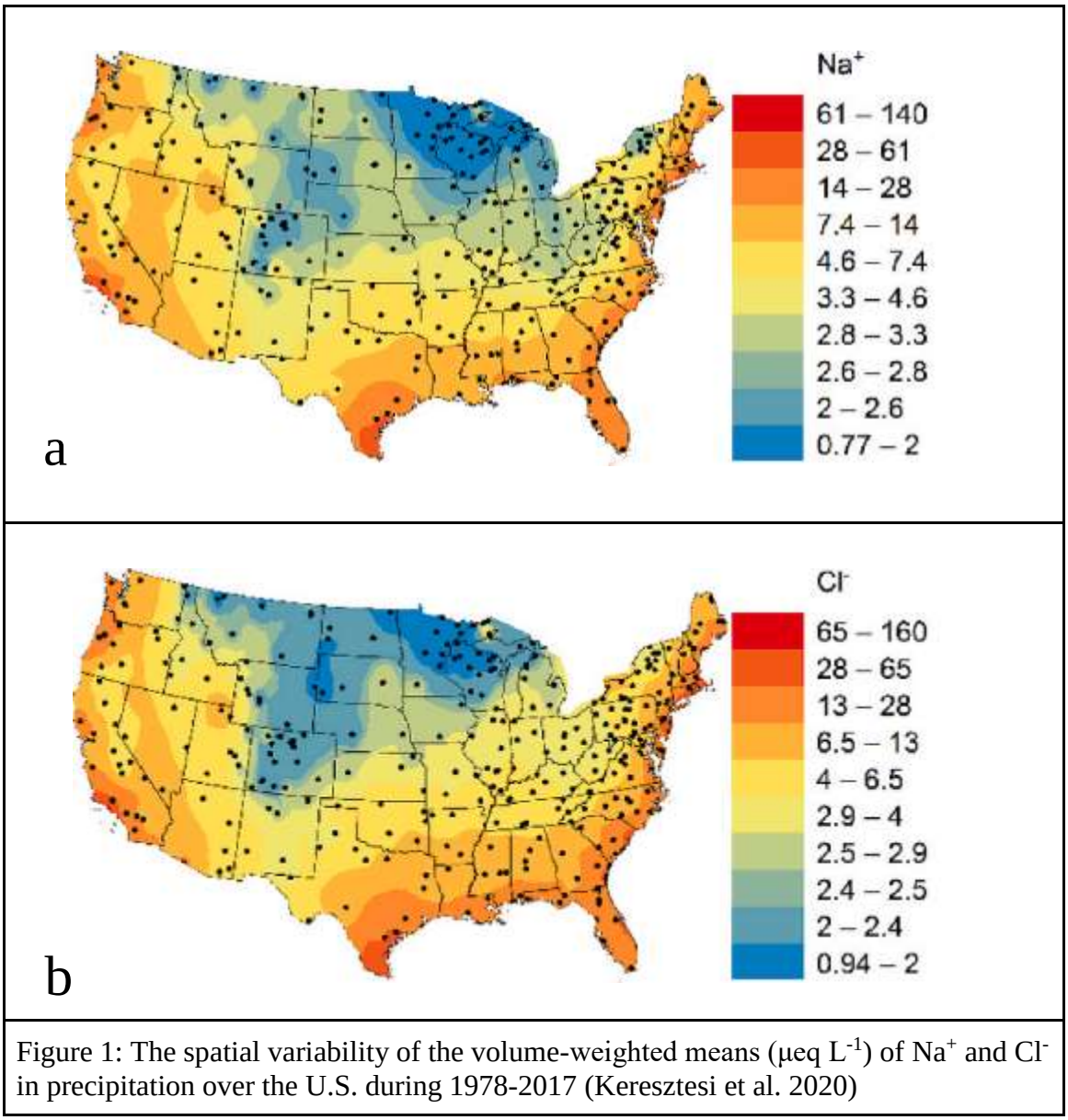

Figure 1: The spatial variability of the volume-weighted means (μeq L^{-1}) of Na^+ and Cl^- in precipitation over the U.S. during 1978-2017 (Keresztesi et al. 2020)

1.3 Nature of Rainfall

Hawai‘i holds a diverse climatology with strong rainfall gradients. On average, the windward side (northeast-facing) of O‘ahu experiences more rainfall than the leeward side due to the interaction between the trade winds and the topography (Figure 2). Northeasterly trade winds blow 60-80% of the time, depending on the season, bringing

clouds and rainfall in primarily from that direction. When the trade winds meet the steep windward topography, the air is lifted, and cloud formations are initiated and enhanced. Because rainfall initiates on the windward side and based on the findings of Keresztesi et al. 2020, we expect that a similar gradient of Na^+ and Cl^- in rainwater exists on Oʻahu as it does across the conterminous U.S. We expect higher concentrations near the coastline near where waves break, and SSA concentrations are high, and smaller concentrations inland or on the leeside.

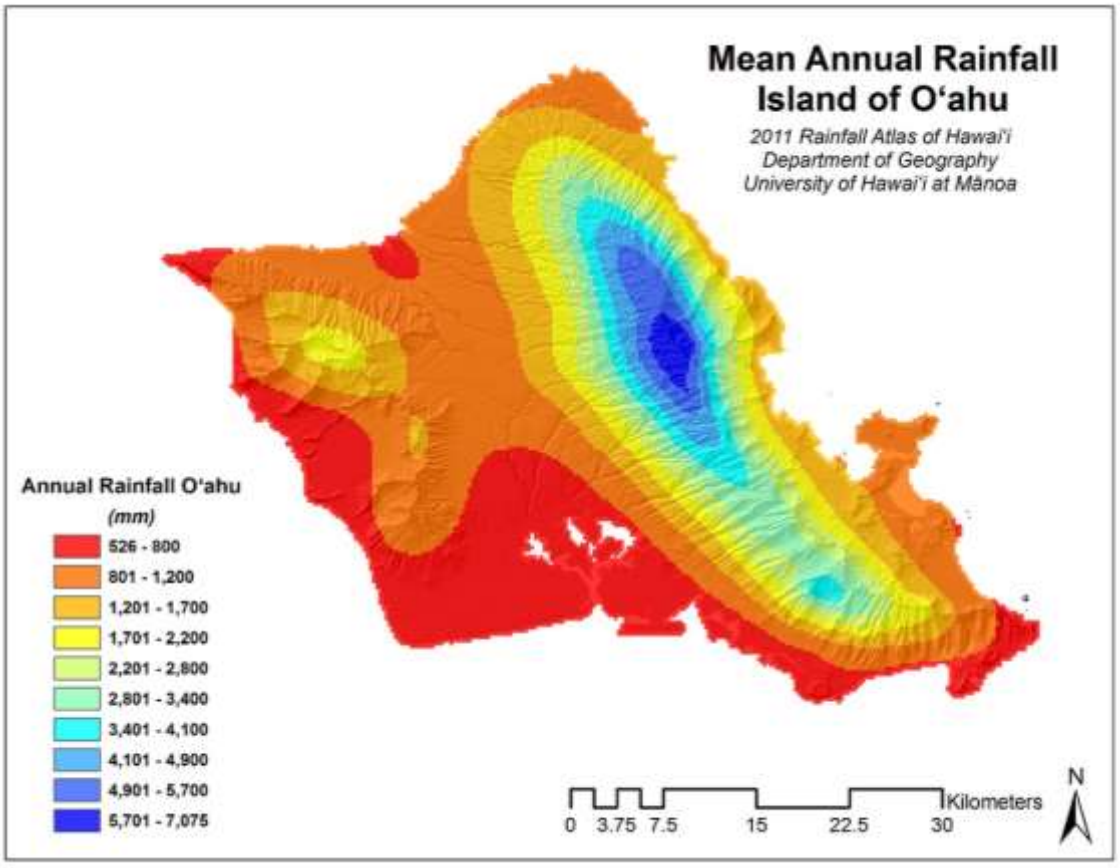

Figure 2: A map of the mean annual rainfall for the island of Oʻahu, produced by the Giambelluca Group at the University of Hawaiʻi at Mānoa (Giambelluca et al. 2013).

2.0 METHODS

2.1 Sampling

The rainwater samples were collected using a Palmex Ltd. rain sampler bucket (Groning et al. 2012) along the windward coast of Oʻahu, as shown by the yellow star in Figure 3a. Sampling took place from the beginning of March 2021 through the end of May 2021, and a total of 41 rain events were collected and analyzed in this study. The utilized rain sampler prevents re-evaporation from occurring through an isolated sampling bottle and tubes running around and within the sampling bottle (Figure 4).

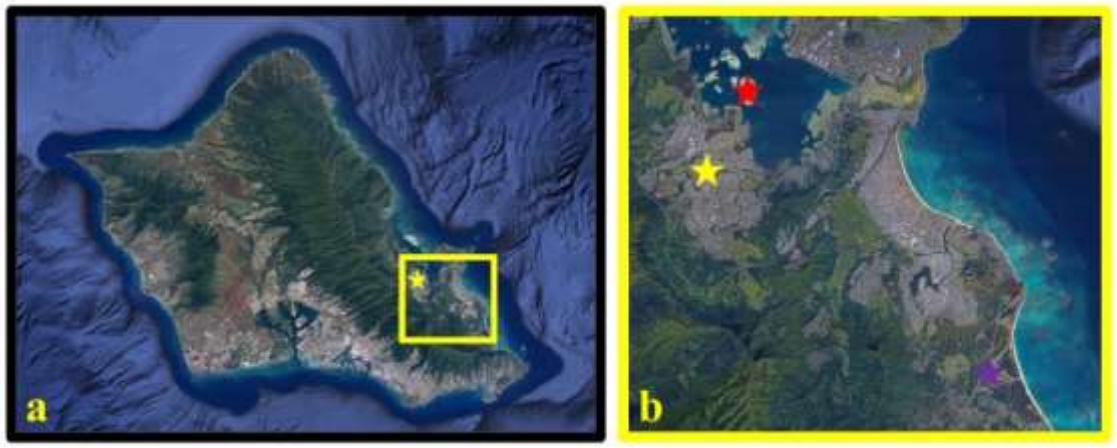

Figure 3. a) is a satellite image of the Island of Oʻahu, while b) represents a zoomed-in portion of the yellow box present in (a). The yellow star marks the sampling location for the rainwater collection in both figures, and the red and purple stars mark the locations of HIMB and Bellows respectively.

Rain samples were collected daily from the rooftop of a home located in Kaneohe, Hawaiʻi. The high collection location ensured that no trees or other obstacles would affect rainwater collection. For storage, 15 mL test tubes were rinsed with deionized water and a small portion of the rainwater samples before filling the tube with the rest of the rain sample to reduce potential contamination. Each part of the rain sampler was disassembled and washed thoroughly using deionized water daily. There was not always

enough rain every day to fill a 15 mL test tube, and in that case, the rain sampler bucket was still cleaned, but no sample was collected.

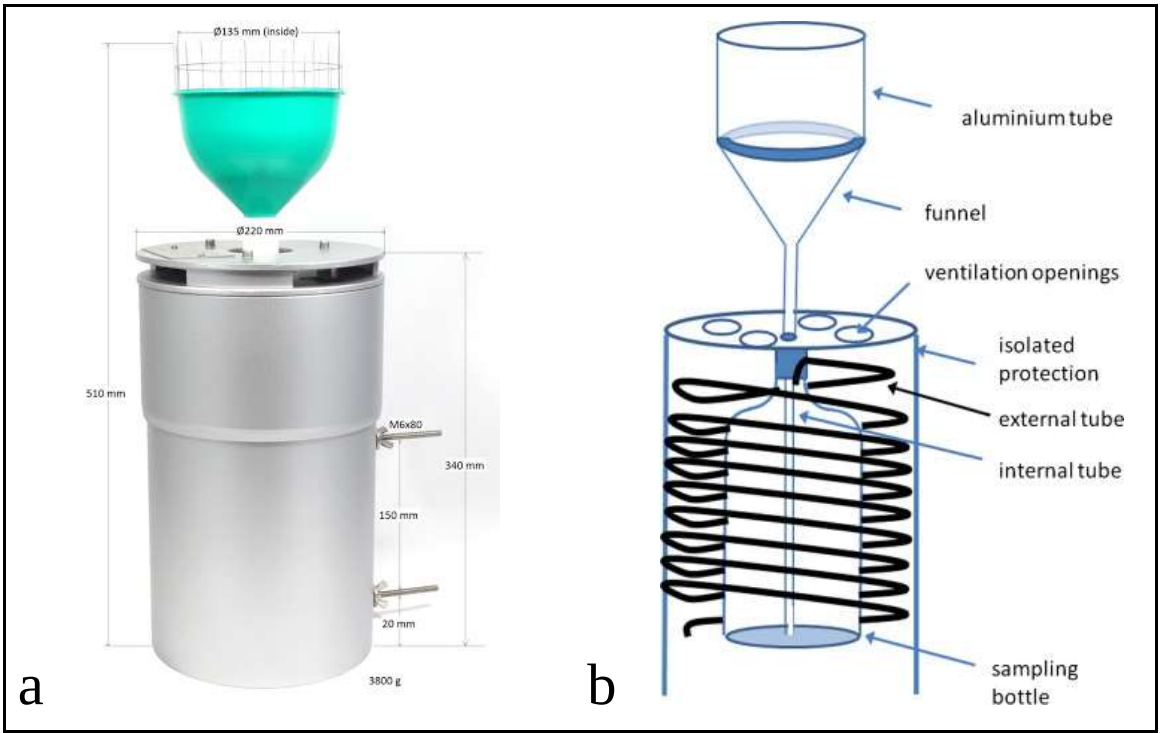

Figure 4. a) shows the Palmex rain bucket assembled with its proper dimensions (Fig. 4 from Groning et al. 2012). b) is a diagram of the Palmex rain sampler bucket demonstrating how it prevents evaporation and heating of the collected rainwater (Fig. 4 from Groning et al. 2012).

2.2 Lab Analysis

Every week, any collected rainwater in the 15 mL test tubes were dropped off for analysis at the Analytical Chemistry lab on the University of Hawai‘i at Mānoa campus, part of the Water Resource Research Center. Major ions were determined using dual Dionex ICS-1100 Ion Chromatographs operated at ambient temperature. Anions were separated on a Dionex IonPac AS14A column with 8 mM Na_2CO_3·/1 mM $NaHCO_3$ eluent. Cations were separated on a Dionex IonPac CS12A column with 20 mM

CH_3SO_3H eluent. The flow rate was 1.0 mL min^{-1}, with detection by suppressed conductivity.

The result of this analysis was measurements of Chloride, Nitrate, Sulfate, Sodium, Ammonium, Potassium, Magnesium, and Calcium for every rainwater sample. The accuracy of each ion measurement is found by the relative standard deviation percentage in Table 1a and 1b. One hundred times cation and ten times anion concentrate were utilized to calculate the relative standard deviation (RSD) respectively. A known concentration of the ion is utilized as the control (ppm) and the results of the run are analyzed against this control. If the measured value varies significantly from the expected value, it is less accurate and has a higher RSD. A lower RSD value correlates with a more accurate measurement.

Table 1a. A comparison of the Ion Chromotograph's readings against the check standard for Cations. A lower RSD value suggests a higher accuracy. Expected (exp) values of each ion (ppm) are included in the top row.

								Exp	0.5	2	2.5	5	2.5	5
Sample Date (YYMMDD)	(mg L^{-1})	Fl	Cl^-	NO_{2-}	Br	NO_{3-}	PO_4^{3-}	SO_4^{2-}	Li	Na^+	NH_4^+	K	Mg	Ca+
210219	100x Cation stnd	n.a.	33.43	n.a.	n.a.	n.a.	n.a.	n.a.	0.50	2.02	2.31	5.10	2.56	5.17
210222	100x Cation stnd	n.a.	32.49	n.a.	n.a.	n.a.	n.a.	n.a.	0.50	2.02	2.30	5.12	2.57	5.19
210226	100x Cation stnd	n.a.	33.48	n.a.	n.a.	n.a.	n.a.	n.a.	0.50	2.01	2.42	5.13	2.56	5.20
210315	100x Cation stnd	n.a.	32.16	n.a.	n.a.	n.a.	n.a.	n.a.	0.49	1.97	2.42	4.97	2.50	5.09
210326	100x Cation stnd	n.a.	33.67	n.a.	n.a.	n.a.	n.a.	n.a.	0.5	2.02	2.40	5.09	2.58	5.10

210402	100x Cation stnd	n.a.	33.78	n.a.	n.a.	n.a.	n.a.	n.a.	0.5	2.02	2.48	5.09	2.58	5.21
210416	100x Cation stnd	n.a.	34.54	n.a.	n.a.	n.a.	n.a.	n.a.	0.5	2.04	2.45	5.17	2.61	5.27
210430	100x Cation stnd	n.a.	32.66	n.a.	n.a.	n.a.	n.a.	n.a.	0.49	1.97	2.40	4.93	2.51	5.08
210507	100x Cation stnd	n.a.	32.42	n.a.	n.a.	n.a.	n.a.	n.a.	0.51	2.04	2.46	5.14	2.58	5.17
210521	100x Cation stnd	n.a.	32.59	n.a.	n.a.	n.a.	n.a.	n.a.	0.51	2.12	2.61	5.31	2.68	5.37
210604	100x Cation stnd	n.a.	29.84	n.a.	n.a.	n.a.	n.a.	n.a.	0.51	2.11	2.50	5.31	2.74	5.60
								Mean	0.51	2.03	2.43	5.12	2.59	5.22
								n	11	11	11	11	11	11
								Rec (%)	101.27	101.55	97.27	102.47	103.53	104.45
								St. dev	0.01	0.05	0.09	0.12	0.07	0.15
								RSD (%)	2.38	2.35	3.55	2.27	2.68	2.88

Table 1b. A comparison of the Ion Chromotograph's readings against the check standard for Anions. A lower RSD value suggests a higher accuracy. Expected (exp) values of each ion (ppm) are included in the top row.

	Exp	2	10	10	10	10	10	10						
Sample Date (YYMMDD)	(mg L^{-1})	Fl	Cl^-	NO_{2-}	Br	NO_{3-}	PO_4^{3-}	SO_4^{2-}	Li	Na^+	NH_4^+	K	Mg	Ca+
210219	10x Anion stnd	2.13	10.36	10.39	10.42	10.4	20.7	10.43	n.a.	30.49	n.a.	7.79	0.05	0.17
210222	10x Anion stnd	2.04	10.01	10.03	10.1	10	20.02	10.07	n.a.	30.2	n.a.	7.75	0.05	0.28
210226	10x Anion stnd	2.09	10.16	10.2	10.25	10.18	20.47	10.32	n.a.	30.04	n.a.	7.7	0.06	0.2

210315	10x Anion stnd	2.04	10.13	10.06	10.19	10.15	20.06	10.23	n.a.	30.13	n.a.	8.04	0.06	0.2
210326	10x Anion stnd	2.05	10.11	10.07	10.12	10.15	20.37	10.12	n.a.	29.54	n.a.	7.97	0.07	0.21
210402	10x Anion stnd	2.04	10.09	10.06	10.1	10.09	20.05	10.2	n.a.	29.54	n.a.	7.89	0.06	0.2
210416	10x Anion stnd	2.09	10.41	10.31	10.41	10.36	20.73	10.53	n.a.	30.34	n.a.	7.79	0.05	0.17
210430	10x Anion stnd	1.97	10.5	10.54	10.49	10.48	20.86	10.54	n.a.	30.83	n.a.	8.07	0.07	0.23
210507	10x Anion stnd	2.08	10.38	10.43	10.35	10.36	20.67	10.46	n.a.	31.88	n.a.	8.29	0.05	0.15
210521	10x Anion stnd	1.95	9.99	9.96	9.99	10.02	20.07	9.83	n.a.	32.14	n.a.	8.45	0.1	0.35
210604	10x Anion stnd	1.84	9.34	9.42	9.34	9.34	18.4	9.28	n.a.	32.43	n.a.	8.86	0.12	0.44
	Mean	2.03	10.13	10.13	10.16	10.14	20.22	10.18						
	n	11	11	11	11	11	11	11						
	Rec (%)	101.45	101.35	101.34	101.6	101.39	101.09	101.83						
	st.dev	0.08	0.31	0.3	0.32	0.31	0.68	0.37						
	RSD (%)	4.02	3.11	2.99	3.1	3.05	3.36	3.63						

2.3 Meteorological Comparison

To place the rainwater samples and solute analysis into context, the atmospheric properties and conditions of each day were compared. Because rainwater was sampled at daily intervals, we also look at daily averages of meteorological conditions including wind speed, wind direction, and rainfall amount. The ion concentrations, as well as rain rate, were compared against environmental data from the Hawaii Institute of Marine Biology (HIMB), shown by the red star in Figure 3, and Bellows Airforce Base

(Bellows), shown by the purple star. Hourly wind from both weather stations was averaged between collection times to get an average wind speed and direction during the time that rain was collected.

All 42 samples were compared to environmental variables such as wind speed, wind direction, air temperature, and rain rate. While wind measurements at HIMB were the closest to the rainwater collection location, the dataset was incomplete and therefore wind data from Bellows was used for all of the comparisons to the wind. Air temperature is also taken from HIMB.

Rain rate was calculated using the total water mass from each 24 hour sampling period divided by the area of the rain collection funnel (14313.88 mm^2). Because 1 g of water equals 1 ml, and 1 ml is 1000 mm^3, the total water mass for a sampling day can be converted into mm day^{-1}, and then divided by 24 hours to yield the rain rate per hour in mm $hour^{-1}$. Equation 2 shows this equation. Computing hourly rain rate allowed for comparison against the HIMB hourly rain rate.

$$\frac{24\ Hour\ Total\ Water\ Mass\ (ml)}{1} * \frac{1000\ mm^3}{1\ ml} * \frac{1}{Area\ of\ funnel\ (mm^2)} * \frac{1}{24} = mm/hr$$

(Equation 2)

2.4 Analysis Methodology

All datasets were analyzed using Python. Missing data is relatively frequent throughout the ion dataset, as not all ions were present in every sample. Missing data is ignored for calculations of averages and correlations, however, further investigation into

this should be conducted in the future as these ions may have been present, but at concentrations too low to be detected.

3.0 RESULTS

Table 2: Chemical Composition of collected Kaneohe rainwater. The date and total water volume (ml) is given, along with Fl, Cl^-, NO_2, Br, NO_{3-}, PO_4^{3-}, SO_4^{2-}, Li, Na^+, NH_4^+, K, Mg, Ca (units ppm), NO_2-N, NO_{3-}-N, NH_4^+-N, TN ions (units mg/L-N), and PO_4^{3-}P (units mg/L-P).

	Total Water Mass (g)	Fl	Cl^-	Br	NO_{3-}	SO_4^{2-}	Na^+	NH_4^+	K	Mg	Ca	NO_{3-}N	NH_4^+-N	TN Ions
210305	77.25	n.a.	20.97	0.11	0.18	1.82	10.45	0.12	0.52	1.24	2.08	0.04	0.09	0.13
210306	33.67	n.a.	17.58	n.a.	0.17	1.99	9.24	0.06	0.48	0.94	1.17	0.04	0.05	0.09
210307	24.3	n.a.	21.14	n.a.	0.19	2.73	11.14	0.11	0.81	1.23	2.06	0.04	0.09	0.13
210308	2184.16	n.a.	2.5	n.a.	n.a.	0.45	1.38	0.02	0.09	0.19	0.39	n.a.	0.02	0.02
210309	397.47	n.a.	10.69	n.a.	0.1	2.01	5.76	0.03	0.23	0.72	0.6	0.02	0.02	0.05
210310	384.97	n.a.	3.11	n.a.	0.25	0.93	1.89	0.02	0.09	0.22	0.58	0.06	0.02	0.07
210311	287.76	n.a.	1.27	n.a.	0.11	0.55	0.89	0.01	0.04	0.1	0.5	0.02	0.01	0.03
210312	469.31	n.a.	2.01	n.a.	n.a.	0.53	1.22	0.01	0.05	0.15	0.18	n.a.	0.01	0.01
210313	332.39	n.a.	8.19	n.a.	n.a.	1.3	4.57	0	0.16	0.57	0.31	n.a.	0	0
210314	109.94	n.a.	7.23	n.a.	0.43	1.22	3.98	0.05	0.15	0.54	0.3	0.1	0.04	0.14
210315	1119.73	n.a.	1.42	n.a.	0.16	0.42	0.8	0.03	0.04	0.13	0.25	0.04	0.02	0.06
210316	137.02	n.a.	16.6	n.a.	n.a.	2.5	9.02	0.01	0.36	1.11	0.44	n.a.	0.01	0.01
210317	207.66	n.a.	10.03	n.a.	0.06	1.5	5.38	0.04	0.2	0.71	0.29	0.01	0.03	0.04
200319	113.84	n.a.	30.92	0.08	0.74	5.75	16.84	0.19	0.61	2.06	0.85	0.17	0.15	0.31
210320	38.99	n.a.	37.1	0.08	0.47	5.05	19.38	0.1	0.77	2.39	0.98	0.11	0.08	0.18
210323	79.11	n.a.	35.98	0.07	0.66	5.7	19.07	0.17	0.7	2.42	1.32	0.15	0.13	0.28
210324	379.24	n.a.	3.16	n.a.	0.12	1.66	1.8	0.01	0.17	0.34	0.75	0.03	0.01	0.03
210330	59.38	n.a.	5.76	n.a.	0.17	1.03	3.04	0.01	0.12	0.4	0.26	0.04	0.01	0.05
210331	53.61	n.a.	7.09	n.a.	0.12	1.19	3.84	0.05	0.22	0.51	0.85	0.03	0.04	0.07

210402	10.14	n.a.	6.17	n.a.	0.05	0.99	3.26	0.01	0.16	0.45	0.49	0.01	0.01	0.02
210403	221.89	n.a.	15.51	n.a.	0.55	2.76	8.17	0.07	0.31	1.06	0.89	0.12	0.05	0.18
210404	31.8	n.a.	28.65	n.a.	1.32	5.22	15.15	0.1	0.63	1.89	1.16	0.3	0.08	0.38
210406	21.34	n.a.	21.44	n.a.	0.23	3.44	11.15	0.07	0.49	1.39	0.88	0.05	0.05	0.11
210408	21.13	n.a.	21.57	n.a.	0.16	3.36	11.23	0.04	0.46	1.41	0.79	0.04	0.03	0.07
210409	63.76	n.a.	12.14	n.a.	0.36	2.12	6.29	0.04	0.26	0.86	0.9	0.08	0.03	0.11
210410	19.94	n.a.	4.05	n.a.	0.38	0.83	2.15	0.06	0.24	0.33	0.96	0.09	0.05	0.13
210411	72.39	n.a.	1.12	n.a.	0.2	0.29	0.6	0.01	0.06	0.11	0.47	0.05	0.01	0.05
210416	55.73	n.a.	2.83	n.a.	0.08	0.4	1.88	0.11	0.41	0.15	1.77	0.02	0.09	0.1
210426	19.55	0.20	13.13	n.a.	1.64	4.45	7.25	0.22	0.67	0.86	4.72	0.37	0.17	0.54
210427	33.15	0.04	3.95	n.a.	0.92	3.17	2.11	0.22	0.19	0.28	1.34	0.21	0.17	0.38
210428	634.61	n.a.	2.41	n.a.	0.25	0.66	1.25	0.05	0.09	0.16	0.68	0.06	0.04	0.10
210429	41.45	n.a.	13.07	n.a.	1.31	2.76	7.24	0.1	0.3	0.84	0.98	0.3	0.08	0.37
210503	26.81	n.a.	9.44	n.a.	0.42	1.63	5.15	0.13	0.23	0.67	0.78	0.09	0.1	0.2
210504	24.03	n.a.	7.53	n.a.	0.3	1.37	4.15	0.02	0.19	0.48	0.56	0.07	0.02	0.08
210505	43.53	n.a.	9.49	n.a.	0.41	1.65	5.13	0.03	0.19	0.59	0.36	0.09	0.02	0.12
210506	71.77	0.01	7.45	0.02	0.4	1.38	4.39	0.09	0.16	0.63	1.95	0.09	0.07	0.16
210509	56.64	0	8.52	0.03	0.21	1.45	4.97	0.07	0.35	0.63	0.58	0.05	0.05	0.1
210515	29.78	0.01	14.05	0.04	0.4	2.34	8.26	0.11	0.55	1.05	1.01	0.09	0.09	0.18
210516	43.16	0	11.94	0.04	0.35	2.06	6.98	0.07	0.32	0.94	0.57	0.08	0.05	0.13
210520	33.21	0.01	10.89	0.03	0.25	1.83	6.68	0.04	0.24	0.9	0.8	0.06	0.03	0.09
210522	39.14	0.01	14.77	0.04	0.58	2.81	9.13	0.09	0.35	1.25	1.69	0.13	0.07	0.2
210530	63.05	0.01	3.77	0.01	0.76	1.09	2.38	0.09	0.16	0.37	2.34	0.17	0.07	0.24

Table 2 includes the total water mass and ion concentration for each day and solute analyzed using an ion chromatograph. NO_{2-}, PO_4^{3-}, PO_4^{3-}-P, and NO_2-N and Li were also measured but were not included in the table due to insufficient ion concentrations. The table shows the raw measured data and visualizes the day to day variability of ion concentrations throughout the study. A semi-strong negative

relationship can be found comparing Na^+ and Cl^- against the total water mass collected. The overall concentrations of the aforementioned ions readily decrease as the total water mass collected increases. This follows the expected pattern as we assumed further rainfall would dilute the initial cloud condensation nuclei being salt. Other ions such as NO_{3}-, SO_4^{2-}, NH_4^+, K, Mg, and Ca follow a very similar relationship in regard to total water mass collected.

Table 3: Major ions composition of rainwater (ppm). The minimum, maximum, average (avg), and standard deviation of total water volume (ml) is calculated, along with Fl, Cl^-, NO_2, Br, NO_{3}-, PO_4^{3-}, SO_4^{2}-, Li, Na^+, NH_4^+, K, Mg, Ca (units ppm).

	Total Water Mass (g)	Fl	Cl^-	Br	SO_4^{2-}	Na^+	NH_4^+	K	Mg	Ca+	NO_{3}-N	NH_4^+-N	TN Ions
Min	10.14	0	1.12	0.01	0.29	0.6	0	0.04	0.1	0.18	0.01	0	0
Max	2184.16	0.2	37.1	0.11	5.75	19.4	0.22	0.81	2.42	4.72	0.37	0.17	0.54
Avg	194.47	0.03	11.59	0.05	2.06	6.3	0.07	0.31	0.79	0.97	0.09	0.05	0.14
St. Dev.	379.319	0.064	9.276	0.031	1.453	4.9	0.057	0.211	0.595	0.805	0.08	0.044	0.119

Table 3 includes the minimum, maximum, and average for each variable measured during the sample analysis. NO_{2}-, PO_4^{3-}, PO_4^{3-}-P, and NO_2-N and Li were also measured but were not included in the table due to insufficient ion concentrations. The concentrations of Cl^- and Na^+ remained dominant while a minute concentration of Fl, Br, NH_4^+-N, and NH_4^+ were found for each rainwater sample. The table significantly condenses the raw data shown in Table 2.

Table 4: This table shows the analyzed ions' R^2 values with respect to one another. The R^2 values are color-coded, with red denoting a positive correlation and blue highlighting a negative correlation. The darker the color, the stronger the correlation.

	Chloride	Sodium	Nitrate	Bromide	Sulfate	Ammonium	Potassium	Magnesium	Calcium	R^2
Chloride	1.000	0.998	0.356	0.968	0.914	0.448	0.882	0.992	0.156	1.000
Sodium		1.000	0.366	0.973	0.916	0.460	0.888	0.996	0.171	0.750
Nitrate			1.000	0.313	0.618	0.716	0.467	0.360	0.652	0.500
Bromide				1.000	0.964	0.695	0.928	0.965	-0.439	0.250
Sulfate					1.000	0.670	0.870	0.915	0.373	0.000
Ammonium						1.000	0.630	0.454	0.675	-0.250
Potassium							1.000	0.870	0.462	-0.500
Magnesium								1.000	0.167	-0.750
Calcium									1.000	-1.000

Table 4 describes the relative correlation between the ion concentrations that were analyzed. As expected, a majority of the ions commonly found in seawater such as Na^+, Cl^-, Br, K, Mg, and SO_4^{2-} hold strong correlations with each other. The relative correlation table can be utilized to determine the possible sources of the measured ions.

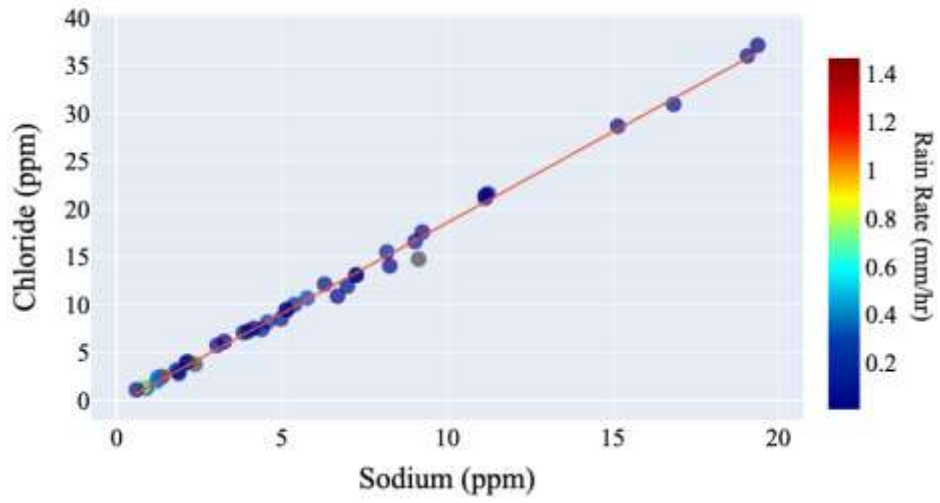

Figure 5. Sodium and Chloride concentrations are compared, with the line of best fit plotted in orange. The colors of the data represent the 24-hour averaged rain rate calculated for that sample day.

In Figure 5, chloride is plotted against sodium with a color scale for rain rate. There is a very strong positive correlation between both ion concentrations. This was expected due to the collection location's proximity to the ocean. There is also a weak relationship between solute concentration and rainfall with higher concentrations having a lower rain rate on average. A portion of the data from table 2 is visualized within the figure above.

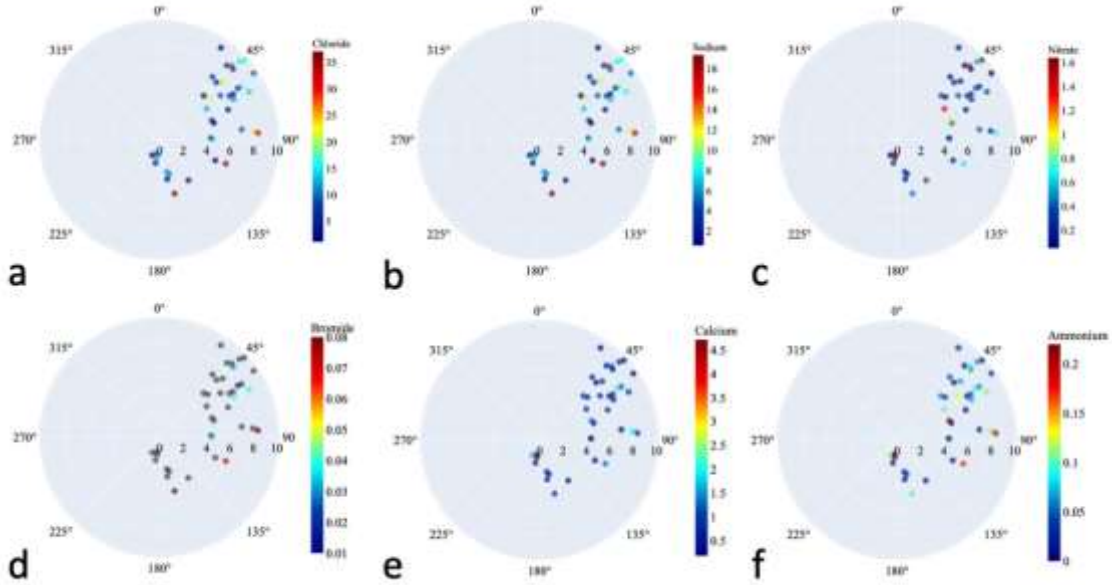

Figure 6. Graphs a-f are wind-rose diagrams, where the angle represents the 24-hour average wind direction and the distance from the center is the 24-hour averaged wind speed in meters per second for each sample day. The colors of each plotted point represent the respective ion concentration taken from that sample for the following ions: a) chloride, b) sodium, c) nitrate, d) bromide, e) calcium, and f) ammonium. Graphs that have grey dots represent samples without that specific ion, such as in d; Bromide was only observed on a few sampling days.

In Figure 6, ions concentration, wind speed, and direction were plotted with a color bar of the designated ion. The wind-rose diagram shows wind speed via distance

from center, and the wind direction through the angle. This table was utilized to find correlations between atmospheric variables and ion concentrations. Throughout each wind-rose diagram, a similar pattern can be found with stronger ion concentrations being found on days with relatively strong trade winds with a few outliers of strong concentration on figure 5e coming from southerly winds.

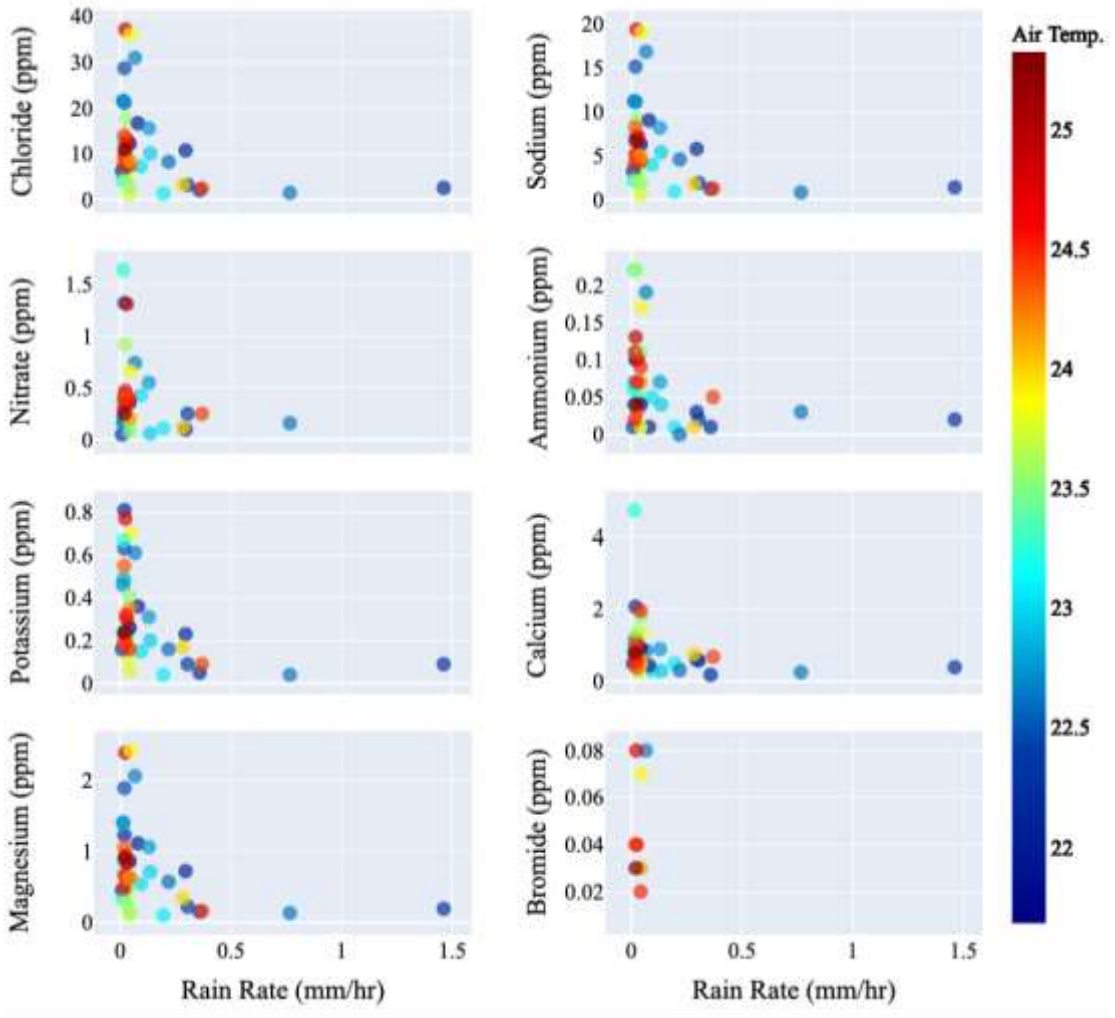

Figure 7: Eight ion concentrations are compared against 24-hour averaged rain rate(mm hr^{-1}). Colors of each sample represent the 24-hour averaged temperature (°C) of that day.

In Figure 7, the analyzed ion concentrations were compared to the average rain rate with a color bar of the 24-hour average temperatures. Each ion held a lower concentration with higher rain rates but the patterns dispersed as the rain rate dissipated. This was expected as we assumed a higher rain rate would correlate with lower ion concentrations, especially with Na^+ and Cl^-. However, the lack of a consistent pattern may suggest that the rain rate is not directly related to the ion concentration.

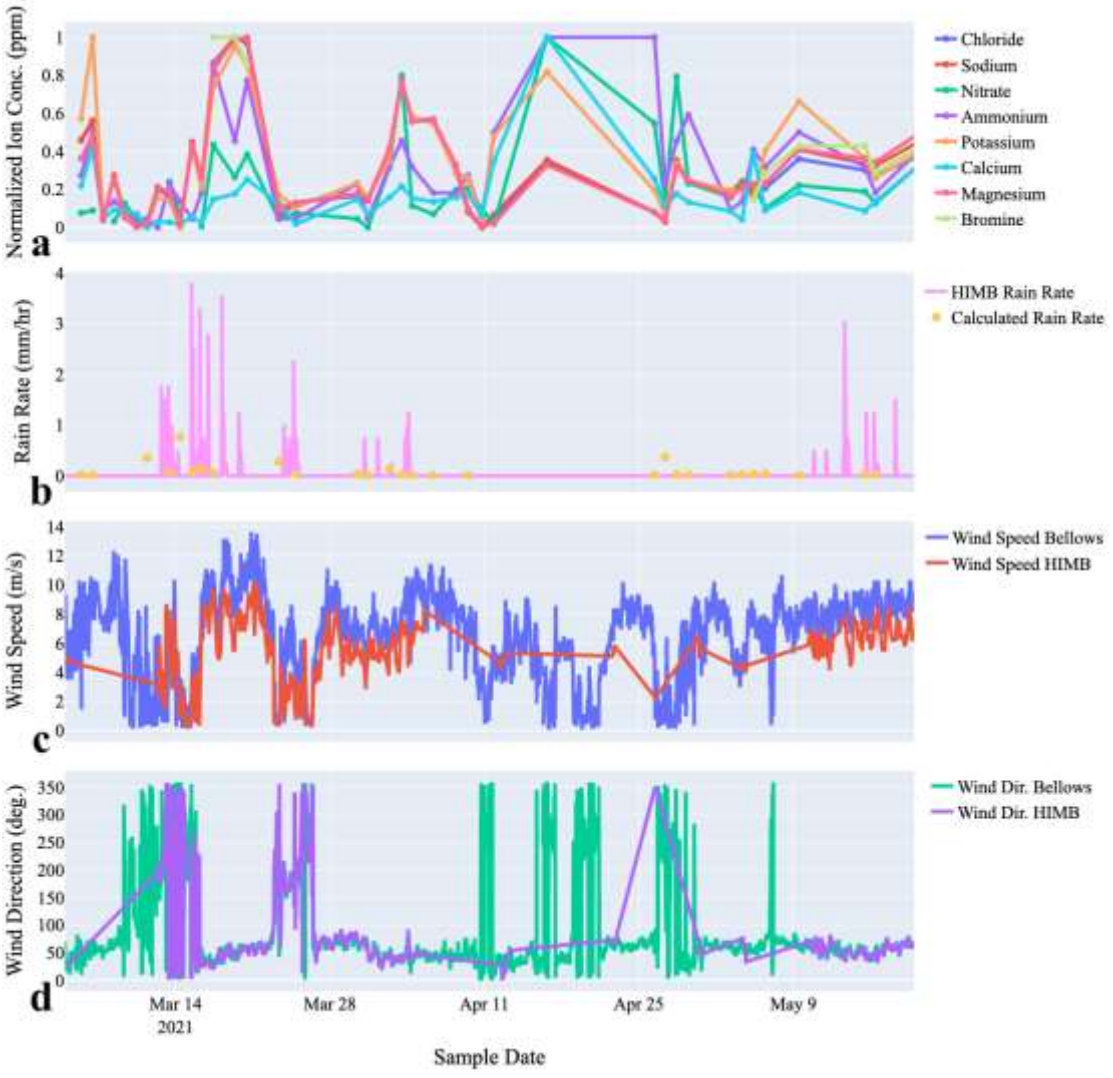

Figure 8: a) shows the variability of ion concentrations between sampling days. The

sampling days are marked by the circle markers, while the lines between them help show how concentrations changed across rain events(mm/hr) for each ion. These values are normalized in order to show how the concentrations changed relative to their minimum and maximum observed values for each ion. b) shows the HIMB and Calculated Rain Rates(mm hr^{-1}) for each day. c) shows the measured 12-meter (U_{12}) and 10-meter (U_{10}) wind speeds(m s^{-1}) for Bellows and HIMB, while d) shows the wind direction (deg.) for those days.

In figure 8, a subplot was created displaying normalized ion concentrations, rain rate, wind speed and wind direction over time. Due to the relatively close proximity, we expected to see the wind speed, direction and rain rate withhold similar values. While wind speed and direction followed the expected pattern, calculated rain rate vastly differed from the HIMB rain rate although these collection locations are in close proximity to each other. Figure 8a and 8c have a semi-strong relationship with increasing ion concentrations correlating similarly with increased wind speed in some cases. Similarly, when comparing figure 8a and 8d, ion concentrations increase on days with trade winds and decrease as wind direction becomes more northerly.

5.0 DISCUSSION and CONCLUSIONS

This study assessed the chemical characteristics of rainwater in Kaneohe, Hawai‘i. Samples were collected daily and taken to the Water Resources Research Center (WRRC) weekly for ion analysis. The ion concentrations were plotted against atmospheric variables to see how wind speed, wind direction, humidity, and rainfall play a role through their modulation of rain processes. Chloride was selected as the reference element to approximate the imprint of marine and non-marine salts on the chemical composition of precipitation since in most of the rain events the Na^+/Cl^- ratio had similar

values compared to the Na^+/Cl^- seawater ratio (Keresztesi et al. 2020). The study found that the concentrations of ions commonly found in seawater strongly correlated with each other. In specific, the strong correlation (R=0.99) between Na^+ and Cl^- suggests that the ions originated from the sea spray and marine salts of the windward coastline. In addition, Na^+ and Cl^- had a very strong correlation with consistent trade winds. The sea spray from the top of breaking waves is picked up through the trade winds and brought to higher altitudes in which it may act as a CCN, rapidly grow, broaden the cloud droplet size distribution, and readily initiate the warm-rain processes (Chen et al. 2007, Jensen and Nugent, 2017). The hypothesis was supported in regards to the decreased ion concentration of Na^+ and Cl^- as total water mass collected increased but due to the lack of precise rain rate at the collection location, a similar pattern was not found between rain rate at the HIMB station and the aforementioned ion concentrations.

On average, our samples contained a relatively significant concentration of Mg and Ca being 0.97 ppm and 0.79 ppm respectively. The presence of $Ca2^+$ and $Mg2^+$ in precipitation shows the influence of terrestrial sources, such as the dissolution of dolomites and limestones (Niu et al. 2014; Szep et al. 2019, 2018; Xiao 2016) but calcium can be originating from anthropogenic activities too, such as open quarries, cement factories, while magnesium can also be attributed to marine sources (Xiao et al. 2017). While quarries are not in abundance across O‘ahu, a small quarry can be found within ~5 miles which may have an influence on the calcium concentrations found in our rain samples. Due to the relatively insignificant environmental footprint of O‘ahu, we expected a small value of ammonium to be found in our samples. This idea was proven

and suggests that anthropogenic sources had little impact on the concentration of ammonium.

Similar findings are expected to be found along the windward coastline with decreased ion concentrations inland especially on the leeside of the Ko'olau mountain range. The mountain range will have a form of blocking effect that can be observed in front of air masses loaded with sea salt, containing high concentrations of chloride and sodium (Keresztesi et al. 2020). Trade winds are common in Hawai'i but the mountainous regions may drastically affect the findings. We expect the ion concentrations of the leeside of the mountains to be drastically different from the windward side. Although samples were collected in a singular location due to time restrictions, samples should be collected in a variety of locations across the island of O'ahu varying from the coastline to inland to improve this study further.

The latter SSA and sulfate aerosol can activate as CCN at low supersaturations in stratus clouds due to their high hygroscopicity. Their increased size when activated facilitates both gas-to-particle conversion and collision coalescence such that they grow to larger dry sizes upon evaporation (Blot et al. 2013). The SSA being activated as a CCN in stratus clouds would result in higher SSA concentrations in passing showers rather than longer rain events from cumulonimbus clouds.

Warm rain is an integral component of the tropical precipitation system, contributing to heating and moistening of the lower troposphere, modifying stability, and possibly altering the recycling time scales of organized tropical convection (Johnson et al. 1999; Johnson and Lin 1997; Mapes 2000; Wu 2003; Del Genio and Kovan 2002).

While the salt concentration in rainwater can have a significant effect on the chemical balances of the landscape, the minute salt concentration may not have a direct influence on a person's daily life right away. In the future, an increase of salt concentration may lead to increased oxidation of common household items. In addition, the increase of SSA activating as a CCN will result in higher rainfall amounts which may lead to natural disasters or further chemical imbalances. The information found within our study can be further analyzed to find the sources of each ion.

To further this study, additional sampling locations should be utilized with a rain gauge included in each. While an analysis against wave height was attempted within the study, the weather stations nearby did not have any wave data to utilize due to the buoys being down for maintenance. A higher salt concentration may be found in days with significant wave heights due to the additional salt from the top of the breaking waves.

LITERATURE CITED

Avery, G. B., Kieber, R. J., Willey, J. D., Shank, G. C., and Whitehead, R. F.: Impact of hurricanes 25 on the flux of rainwater and Cape Fear river water dissolved organic carbon to Long Bay, Southeastern US, Glob. *Biogeochem. Cy.*, 18, 3015–3020, 2004.

Barbieri, M. 2016. The importance of enrichment factor (EF) and geoaccumulation index (Igeo) to evaluate the soil contamination. *J. Geol. Geophys* 5.1: 1-4.

Blot, R., A. D. Clarke, S. Freitag, V. Kapustin, S. G. Howell, J. B. Jensen, L. M. Shank, C. S. McNaughton, and V. Brekhovskikh 2013. Ultrafine sea spray aerosol over the southeastern Pacific: open-ocean contributions to marine boundary layer CCN. *Atmospheric Chemistry and Physics* 13.14: 7263-7278.

Chen, C.-W., Kao, C.-M., Chen, C.-F., & Dong, C.-D. (2007). Distribution and accumulation of heavy metals in the sediments of Kaohsiung Harbor, Taiwan. *Chemosphere*, 66(8), 1431–1440

Del Genio, A. D., and W. Kovan, 2002. Climatic properties of tropical precipitating convection under varying environmental conditions, *J. Clim.*, 15, 2597 – 2615.

Eriksson, E. 1957. The Chemical Composition of Hawaiian Rainfall, *Tellus*, 9:4, 509-520, DOI: 10.3402/tellusa.v9i4.9125

Giambelluca, T.W., Q. Chen, A.G. Frazier, J.P. Price, Y.-L. Chen, P.-S. Chu, J.K. Eischeid, and D.M. Delparte, 2013: Online Rainfall Atlas of Hawai‘i. *Bull. Amer. Meteor. Soc.* 94, 313-316, doi: 10.1175/BAMS-D-11-00228.1.

Greaver, T.L., Sullivan, T.J., Herrick, J.D., Barber, M.C., Baron, J.S., Cosby, B.J., Deerhake, M.E., Dennis, R.L., Dubois, J.J.B., Goodale, C.L., Herlihy, A.T., Lawrence, G.B., Liu, L., Lynch, J.A., Novak, K.J., 2012. Ecological effects of nitrogen and sulfur air pollution in the US: what do we know? *Front. Ecol. Environ*. 10, 365–372. https://doi.org/10.1890/110049.

Gröning, M., H.O. Lutz, Z. Roller-Lutz, M. Kralik, L. Gourcy, L. Pöltenstein,. 2012. A simple rain collector preventing water re-evaporation dedicated for δ18O and δ2H analysis of cumulative precipitation samples. *Journal of Hydrology* 448: 195-200.

Jensen, J. B., and A. D. Nugent. 2-17. Condensational growth of drops formed on giant sea-salt aerosol particles. *Journal of Atmospheric Sciences* 74.3, 679-697.

Johnson, R. H., T. M. Rickenbach, S. A. Rutledge, P. E. Ciesielski, and W. H. Schubert, 1999. Trimodal characteristics of tropical convection, *J. Clim*., 12, 2397 – 2418.

Johnson, R. H., and X. Lin, 1997. Episodic trade wind regimes over the western Pacific warm pool, *J. Atmos. Sci.*, 54, 2020 – 2034.

Keresztesi, A., Birsan, M.-V., Nita, I.-A., Bodor, Z., Szep, R., 2019a. Assessing the neutralisation, wet deposition and source contributions of the precipitation chemistry over Europe during 2000–2017. *Environ. Sci. Eur*. 31 (50) https://doi. org/10.1186/s12302-019-0234-9.

Keresztesi, Á., I.-A. Nita, R. Boga, M.-V. Birsan, Z. Bodor, and R. Szép, 2020. Spatial long-term analysis of rainwater chemistry over the conterminous United States. *Environmental Research* 188: 109872.

Lau, K. M., and H. T. Wu. 2003. Warm rain processes over tropical oceans and climate implications. *Geophysical Research Letters* 30.24.

Lehmann, C.M.B., Bowersox, V.C., Larson, S.M., 2005. Spatial and temporal trends of precipitation chemistry in the United States, 1985-2002. *Environ. Pollut*. 135, 347–361. https://doi.org/10.1016/j.envpol.2004.11.016.

Mullaugh, K. M., J. D. Willey, R. J. Kieber, R. N. Mead, and G. B. Avery Jr. 2012. Dynamics of the chemical composition of rainwater throughout Hurricane Irene. *Atmospheric Chemistry & Physics Discussions* 12.10.

Mapes, B. E., 2000, Convective inhibition, subgrid scale triggering energy, and stratiform instability in a toy tropical wave model, *J. Atmos. Sci.*, 57, 1515 – 1535.

Niu, H., He, Y., Lu, X.X., Shen, J., Du, J., Zhang, T., Pu, T., Xin, H., Chang, L., 2014. Chemical composition of rainwater in the Yulong snow mountain region, southwestern China. *Atmos. Res*. 144, 195–206. https://doi.org/10.1016/j. atmosres.2014.03.010.

Szep, R., Bodor, Z., Miklossy, I., Nița, I.A., Oprea, O.A., Keresztesi, A., 2019. Influence of peat fires on the rainwater chemistry in intra-mountain basins with specific atmospheric circulations (Eastern Carpathians, Romania). *Sci. Total Environ*. 647, 275–289. https://doi.org/10.1016/j.scitotenv.2018.07.462.

Wu, Z., 2003. A shallow CISK, deep equilibrium mechanism for the interaction between large-scale convection and circulation in the tropics, *J. Atmos. Sci*., 60, 377 – 392.

Wang, W., Xu, W., Collett, J.L., Liu, D., Zheng, A., Dore, A.J., Liu, X., 2019. Chemical compositions of fog and precipitation at Sejila Mountain in the southeast Tibetan Plateau, *China. Environ. Pollut*. 253, 560–568. https://doi.org/10.1016/j. Envpol.2019.07.055.

Xiao, H.-Y., Shen, C.-Y., Xiao, H.-W., Chen, L., Luo, L., Long, Z.-H., Li, D.-N., Long, A.-M., 2017. Atmospheric aerosol compositions over the South China Sea: temporal variability and source apportionment. *Atmos. Chem. Phys*. 17, 3199–3214. https://doi.org/10.5194/acp-17-3199-2017.

Xiao, J., 2016. Chemical composition and source identification of rainwater constituents at an urban site in Xian. *Environ. Earth Sci.* 75, 1–12. https://doi.org/10.1007/ s12665-015-4997-z.

Zunckel, M., Saizar, C., Zarauz, J., 2003. Rainwater composition in northeast Uruguay. Atmos. Environ. Times 37, 1601–1611. https://doi.org/10.1016/S1352-2310(03) 00007-4.